J Supercond Nov Magn (2017) 30:331–341
DOI 10.1007/s10948-016-3726-5

ORIGINAL PAPER

Upper Critical and Irreversibility Fields in $Ba(Fe_{0.95}Ni_{0.05})_2As_2$ and $Ba(Fe_{0.94}Ni_{0.06})_2As_2$ Pnictide Bulk Superconductors

Martin Nikolo[1] · John Singleton[2] · Dmitry Solenov[1] · Jianyi Jiang[3] · Jeremy D. Weiss[3] · Eric E. Hellstrom[3]

Received: 12 July 2016 / Accepted: 13 August 2016 / Published online: 5 September 2016

Abstract A comprehensive study of upper critical and irreversibility magnetic fields in $Ba(Fe_{0.95}Ni_{0.05})_2As_2$(large grain and small grain samples) and $Ba(Fe_{0.94}Ni_{0.06})_2As_2$, polycrystalline bulk pnictide superconductors was made in pulsed fields of up to 65 T. The full magnetic field-temperature ($H - T$) phase diagrams, starting at 1.5 K, were obtained. The higher temperature, upper critical field H_{c2} data are well described by the one-band Werthamer, Helfand, and Hohenberg (WHH) model. The large values of the Maki parameter α indicate that the Zeeman pair breaking dominates over the orbital pair breaking and spin-paramagnetic pair-breaking effect is significant in these materials. At low temperatures, the experimental data depart from the fitted WHH curves, suggesting an emergence of a new phase that could be attributed to the Fulde-Ferrell-Larkin-Ovchinnikov (FFLO) state. Possible multi-band structure of these materials is lumped into effective parameters of the single-band model.

Keywords Upper critical magnetic field · Irreversibility magnetic field · Superconductors · Pnictides · Radio frequency proximity detector oscillator (PDO) measurement

✉ Martin Nikolo
nikolom@slu.edu

[1] Department of Physics, Saint Louis University, St. Louis, MO 63103, USA

[2] National High Magnetic Field Laboratory, Los Alamos National Laboratory, Los Alamos, NM 87545, USA

[3] Applied Superconductivity Center, National High Magnetic Field Laboratory, Florida State University, Tallahassee, FL 32310, USA

1 Introduction

The discovery of superconductivity in compounds containing iron was surprising because magnetism and superconductivity are supposedly opposed phenomena [1]. Elemental iron is a ferromagnet, and many iron compounds exhibit magnetic order [2]; consequently, it was thought that the magnetic nature of iron would disrupt or break apart Cooper pairs [1]. Subsequent research has revealed that superconductivity is enabled by chemical doping of antiferromagnetic parent compounds, with magnetic fluctuations perhaps having a role in stabilizing the superconducting ground-state [1]. The parent compound in iron-based pnictides is semi-metallic, in contrast to the Mott insulator in copper based superconductors [3–7]. Moreover, though, like the cuprates, the iron pnictides are layered with electronically active Fe-As layers alternating with "buffer" layers of different chemical composition [5], they exhibit much lower electronic and superconducting anisotropy [3, 8, 9]. Considering their generally lower critical temperatures compared to the cuprates, the Fe compounds have relatively high upper critical fields and critical current densities, suggesting a variety of future applications [3, 8, 9]. It is clearly of importance to understand the physics that restricts the upper critical fields and critical current densities for polycrystalline samples subject to the helium temperatures that will be employed for many practical applications, and that is the motivation of the current paper.

The upper critical field, $\mu_0 H_{c2}$, is one of the fundamental parameters in type II superconductors and provides important insight into the Cooper-pair-breaking mechanisms in a magnetic field [10–13]. Since the Fe-based superconductors have large upper critical fields, there are not many facilities where high H_{c2}s can be measured at low temperatures; attempts to extrapolate the higher temperature

$H_{c2}(T)$s to low temperatures usually overestimate the actual values [14, 15]. Measurements in large (>50 T) magnetic fields are therefore needed to understand the low-temperature $H_{c2}(T)$ behavior [16]. In this context, it is useful to review briefly how magnetic field breaks the Cooper pairs in superconductors. There are two distinct ways to induce pair-breaking in type-II superconductors by an applied magnetic field—by orbital or spin paramagnetic effects [10, 11]. An external magnetic field that destroys the Cooper pairs by the orbital pair breaking is linked to the appearance of Abrikosov vortex lines [10, 11]. The Lorentz force acts via the charge on the paired electrons and the kinetic energy of the superconducting currents around the vortex cores reduce the superconducting condensation energy [10, 11]. The orbital limiting field is given as $H_{c2}^{\rm orb} = \Phi_0/2\pi\xi^2$ at which the vortex cores begin to overlap; here, Φ_0 is the flux quantum and ξ is the coherence length [10, 11].

On the other hand, the spin paramagnetic pair breaking is a result of the Zeeman effect which aligns the spins of two electrons with the applied field [10, 11]. The spin-paramagnetic pair-breaking effect comes from the Zeeman splitting of spin singlet Cooper pairs. The spin structure is not affected until the Zeeman energy is strong enough to flip one spin of the singlet and break the Cooper pair. This is also known as the Pauli paramagnetic limit or Pauli pair breaking [10, 11]. The Pauli-limiting field $H_{c2}^{\rm P}$ is derived from the condition that the Zeeman energy in the normal state compensates the superconducting condensation energy under magnetic fields [10, 11].

The relative importance of the orbital and paramagnetic effects in the suppression of the superconductivity is described by the Maki parameter $\alpha = \sqrt{2}\, H_{c2}^{\rm orb}/\, H_{c2}^{\rm P}$ where α is of the order of Δ/ε_F, and ε_F is the Fermi energy [17]. In most superconductors, the Maki parameter is usually much less than unity and this indicates that the influence of the paramagnetic effect is negligibly small [17]. However, in materials with heavy electron effective mass, in which the Fermi energy is small, or in layered materials in a magnetic field parallel to the layers, α can be larger than unity [10–13].

For a BCS superconductor where $2\Delta(0) = 3.52k_BT_c$, $H_{c2}^{\rm P}(0)$ becomes $H_{c2}^{\rm P}(0) = 1.84T_c$, where Δ is the superconducting gap energy. The observed $H_{c2}(0)$s in many pnictide compounds significantly exceed the BCS paramagnetic limit $H_{c2}^{\rm P}(0) = 1.84T_c$ above which the pair-breaking Zeeman energy exceeds the binding energy of the Cooper pair [10, 11, 17]. The $H_{c2}(T)$ plots in 122, 111, and 11 (122 stands for $BaFe_2As_2$, 111 for AFeAs, where A is a metal such as Na, Li, etc., and 11 for $FeSe_{1-x}Te_x$) compounds show a steep increase of $H_{c2}(T)$ near T_c followed by the flattening of $H_{c2}(T)$ at lower T [8–18]. This indicates that the Zeeman pair breaking may dominate over the orbital pair breaking, and the Maki parameter $\alpha = \sqrt{2}\, H_{c2}^{\rm orb}/\, H_{c2}^{\rm P} > 1$ [10, 11, 17–19].

Bearing in mind imminent technological applications of Fe-based superconductors at helium temperatures [8, 9, 20–22], in the present work, we apply very high magnetic fields to polycrystalline samples of Fe-based superconductors to assess which of the above mechanisms dominates their low-temperature performance. By fitting the temperature dependence of the upper critical field, we derive descriptive constants such as the Maki parameter and assess how these vary with Ni doping, as we search for clues as to possible future enhancements of these materials.

2 Methods

2.1 Fitting the Temperature Dependence of the Upper Critical Field

Orbital effects on the temperature dependence of the upper critical field $H_{c2}(T)$ were first considered by Helfand and Werthamer (HW). Their methods have been used routinely to analyze data on new superconductors with strongly anisotropic Fermi surfaces and order parameters, despite the fact that HW considered only the isotropic s-wave spherical symmetry of the Cooper pair [10, 11]. In a second paper, Werthamer, Helfand, and Hohenberg (WHH) added the effects of both Pauli paramagnetism and spin–orbital scattering to predict the universal behavior of the upper critical field $H_{c2}(T)$ in superconductors with weak electron-phonon coupling [10, 11]. The WHH approach incorporates both orbital and paramagnetic effects in the upper critical field's temperature dependence by approximately evaluating the non-local non-magnetic and spin-orbit scattering integrals that enter the self-consistent equation for the gap function,

$$\Delta(\mathbf{r}) \ln T_c = \Delta(\mathbf{r}) \ln T + \int d\mathbf{r} K(\mathbf{r}, \mathbf{r}'; H)\Delta(\mathbf{r}'). \quad (1)$$

Here, all the details involving interactions responsible for superconducting instability enter via T_c and the magnetic field; scattering from disorder is introduced via kernel K. This eigenfunction equation has a solution below $H = H_{c2}$. In the dirty limit, when the overall mean free time τ is much less then $1/T$ in units with $k_B = 1$, WHH demonstrated [1] that the critical field is found by setting

$$f(t, h; \alpha, \lambda_{so}) = \ln t + \sum_{n=-\infty}^{\infty} \left\{ \frac{1}{|2n+1|} - \left[|2n+1| + \frac{h}{t} + \frac{(\alpha h/t)^2}{|2n+1| + (h+\lambda_{so})/t} \right]^{-1} \right\} \quad (2)$$

to zero, i.e., $f(t, h; \alpha, \lambda_{so}) = 0$. The dimensionless parameters are defined as

$$t = T/T_c, \quad h = eH_{c2}v_F^2\tau/3\pi T_c$$
$$\alpha = 3/2mv_F^2\tau, \quad \lambda_{so} = 1/3\pi T_c\tau_{so}, \tag{3}$$

where v_F is the Fermi velocity and τ_{so} is the mean free time due to spin-orbit scattering; the parameter λ_{so} describes the strength of the spin–orbit scattering.

Although it is perhaps questionable as to whether the pnictide superconductors approach the dirty limit, a number of workers have used the WHH formalism to fit their $H_{c2}(T)$ data [23–26]. For FeTeSe and FeTeS single-crystal superconductors, the Maki parameters are larger than 1. For FeTeS with $T_c \approx 8$ K and $H_{c2}(0) \approx 28$ T, good fits were obtained using the WHH parameters $\alpha \approx 3$–4 and $\lambda_{so} \approx 0.5$–1, while for FeTeSe with $T_c \approx 15$ K and $H_{c2}(0) \approx 50$ T, the parameters were $\alpha \approx 4$–5 and $\lambda_{so} \approx 1$ [23–25]. Therefore, in the WHH-one band scheme, the relative strength of the spin-paramagnetic effect over the orbital-limiting effect tells us that spin-paramagnetic pair-breaking effect is dominant.

However, in many pnictides, the situation is complicated by the mild anisotropy of the upper critical field [26] and other effects that lead to a variety of different temperature dependences. For instance, 1111 pnictides (ReFeAsO$_{1-x}$F$_x$) typically have convex $H_{c2}(T)$ curves for $H||c$-axis [20, 21] consistent with the behavior expected from the orbitally limited H_{c2}. At the same time, the *concave* shape of $H_{c2}(T)$ curves measured in in KFe$_2$As$_2$, BaFe$_2$As$_2$, Fe$_{1+y}$Se$_x$Te$_{1-x}$, K$_{0.8}$Fe$_{1.76}$Se$_2$, and LiFeAs [23, 25, 28–34], suggests that there is an enhanced role of the Pauli pair breaking. Ghannadzadeh et al. measured upper critical fields of NaFe$_{1-x}$Co$_x$As single crystals in fields parallel and perpendicular to the ab planes [35]. The $H_{c2}(T)$ data were fitted to the WHH model. For fields parallel to the *ab* planes, $H_{c2}(T)$ is well described by the WHH model across all temperatures. However, for field perpendicular to the *ab* planes, the WHH model fitted the data only close to T_c; at lower temperatures, the upper critical field grew at a faster rate. A similar effect was noted by Yuan [36] et al.; for H perpendicular to the ab planes, H_{c2} followed an almost linear increase with decreasing temperatures.

The departure from the typical WHH convex $H_{c2}(T)$ curves has been attributed to two possible mechanisms. Ghannadzadeh et al. [35] suggested that the upward curvature in $H_{c2}(T)$ for perpendicular fields is due to the multiband nature of the superconductivity, as is thought to be the case for the rare-earth 1111 systems (ReFeAsO$_{1-x}$F$_x$ where Re is a rare-earth atom) [20, 21, 26], the 122 systems (BaFe$_2$As$_2$) [27], and the closely related 111 superconductor LiFeAs [20], among others. Comparison with measurements of MgB$_2$ suggests that pnictide superconductors have multiple bands contributing to superconductivity; [20, 37] though in the case of the pnictides, the enhancement of H_{c2} over BCS expectations is relatively much greater, perhaps unrealistically greater for such a model, than in MgB$_2$. Rather, the large enhancement over the orbital pair breaking which limits $H_{c2}(T)$ in conventional superconductors indicates that pnictides may be close to the Fulde–Ferrell–Larkin–Ovchinnikov (FFLO instability [38, 39].

The FFLO instability for which the Zeeman splitting causes a nonzero momentum of the Cooper pairs and spatial oscillations of the superconducting order parameter [38, 39] has been suggested as a possible phase in pnictide compounds. For the FFLO phase to appear, the orbital pair breaking effect must be weak relative to the Pauli paramagnetic effect. In particular, orbital pair breaking, when the vortices induced by the magnetic field overlap in space, has to be weaker, which is not the case for conventional superconductors. Materials with large effective electron masses or layered materials (with quasi-two-dimensional electrical conduction) are candidates for the FFLO state. Spatial modulation of the gap function of the form $c_1e^{i\mathbf{Qr}} + c_2e^{-i\mathbf{Qr}}$ offsets the transition to the normal (paramagnetic) state to higher magnetic fields [20, 27]. Calculations show that in anisotropic superconductors, the FFLO state might lead to an enhancement of the upper critical field H_{c2} to between 1.5 and 2.5 times the Pauli paramagnetic limit [40–42]. Evidence of the FFLO state has been found in heavy fermion [43–46] and organic [47–50] superconductors.

In polycrystalline samples such as ours—i.e., those that will be employed in technological applications—the anisotropy of the superconductivity seen in single crystals will nevertheless be manifested. Proximity effect arguments [51] suggest that whichever is the higher of the critical fields (parallel or perpendicular to the ab planes) at a particular temperature will dominate the behavior of polycrystals. Using the precedent of single-crystal measurements [35, 36], we expect that the WHH fit will work well close to T_c, but that the emergence of any quasi-linear enhancement (which almost always yields a higher critical field) will take over at lower temperatures. Thus, in the analysis below, we develop and use the WHH model to fit data from our polycrystalline samples and make a qualitative assessment of the lower temperature linear deviation. The parameters extracted from WHH allow us to speculate whether the quasi-linear deviations at low temperatures are due to the FFLO state or not.

2.2 Experimental Details

We measured three different Ni-doped samples—two Ba(Fe$_{0.95}$Ni$_{0.05}$)$_2$As$_2$ (Ni5) polycrystalline samples of different average grain size and one Ba(Fe$_{0.94}$Ni$_{0.06}$)$_2$As$_2$ (Ni6). The average grain size of the first Ni5 sample was about 17 μm and its T_c was 19.2 K; the average grain size of

the other Ni5 sample was larger and its T_c was 20.4 K. We label the larger grain and higher T_c sample as Ni5(LG) and the smaller grain and lower T_c sample as Ni5(SG). Ni5(LG) had very low grain connectivity and large grain size, and some FeAs impurities were observed between most grains.

The third Ni-doped sample that we measured was a $Ba(Fe_{0.94}Ni_{0.06})_2As_2$ (Ni6) polycrystalline sample whose T_c was 18.5 K. The parallelepiped dimensions of the samples were as follows: Ni5(LG) $0.7 \times 0.7 \times 2$ mm^3, Ni5(SG) $0.6 \times 0.75 \times 3.9$ mm^3, and Ni6 $0.7 \times 0.7 \times 2$ mm^3, respectively. The cross-sectional areas were chosen to minimize heating caused by the rapidly changing pulsed magnetic fields after several trial experiments.

The samples were synthesized at the Applied Superconductor Center (at the National High Magnetic Field Laboratory), where Ba, Fe, Ni, and As were mixed together, wrapped with Nb foil, and then sealed in a stainless steel vial. The sealed samples were heat treated under a pressure of 193 MPa at 1120 ° C for 12 h, cooled to 900 ° C at the rate of 4 ° C/h, held at 900 ° C for 12 h, and then cooled to room temperature at 150 ° C/h. The phase purity of the samples was checked by powder X-ray diffraction (XRD) [52]. The samples contained a small amount (a few %) of FeAs impurities. The present paper supplements our previous magneto-transport and ac susceptibility work on the same samples [14, 15, 53, 54], taking the samples to much higher fields and much lower temperatures.

Upper critical fields were measured in pulsed magnetic fields of up to 65 T at the National High Magnetic Field Laboratory (NHMFL) campus in Los Alamos, NM. A radio frequency proximity detector oscillator (PDO) induction technique was used, in which the sample is placed inside a coil that forms part of a tank circuit whose resonance frequency is monitored as a function of field and temperature [55, 56]. The exclusion of flux by the sample from the coil (due either to superconductivity or the normal-state skin depth) decreases the inductance of the circuit; hence, the resonant frequency increases. The resonant frequency in a resonant LC tank circuit is given by $f_0 = 1/(2\pi\sqrt{(LC)})$ where L is the circuit's inductance and C the capacitance, respectively. The superconducting-normal state phase transition is observed as a large change in resonant frequency. The circuit is also sensitive to changes in dissipation; features are also observed in the frequency at the lower critical field (which will not be treated in the present paper) and the irreversibility field.

The sample and coil were placed at the field center of a pulsed magnet within a simple double-wall refrigerator inside a liquid ^{4}He bath. This allowed us to reach temperatures as low as 1.38 K, using either ^{3}He or ^{4}He as an exchange medium. For temperatures below 4 K, the samples were immersed in liquid. The samples were also heat-sunk to a large sapphire slab to give extra cooling. Great care was taken to exclude the effects of sample heating due to the rapidly changing field; to this end, experiments were carried out in both the 60-T long-pulse ($dB/dt \sim 100$ T/s) and the 65-T short-pulse ($dB/dt \sim 6000$ T/s) magnets at Los Alamos; a typical pulse shape of the latter is shown in Fig. 1a.

The radio frequency output of the PDO circuit is ~30 MHz; this is down-converted using a double heterodyne system to ~ 2 MHz, allowing the signal to be digitized at 10–20 M samples/s. A discrete Fourier transform (window width 20 μs) is then run on the digitized data to calculate the frequency f as a function of time; the Fourier transform window was applied every 10 μs [55, 56]. In our measurements, the change in frequency at the upper critical field, Δf, was about 350 kHz for the Ni5 samples and

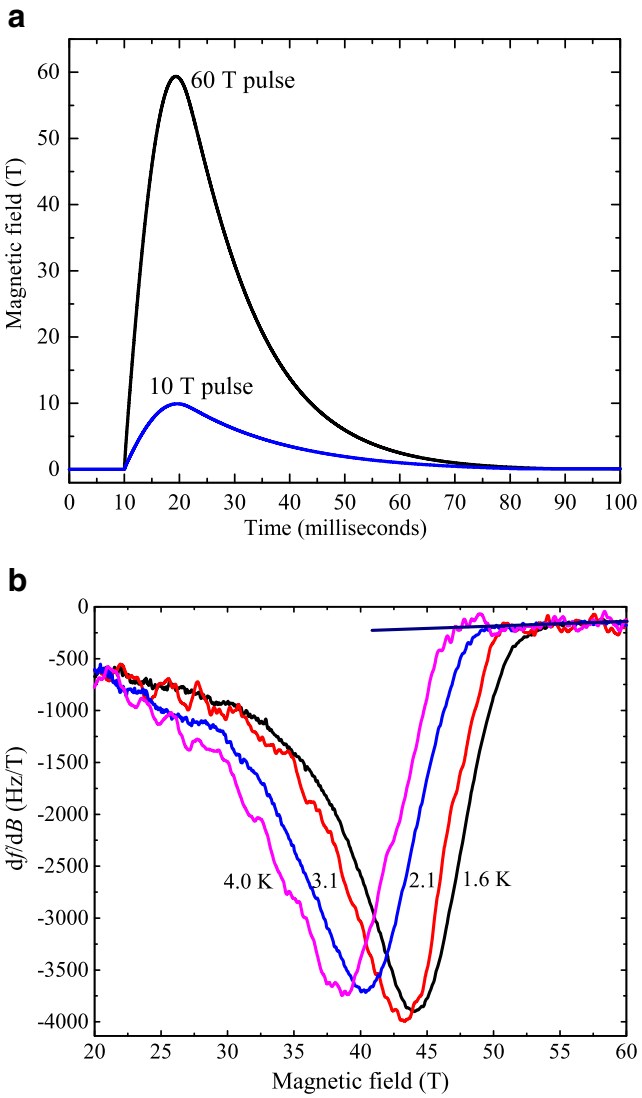

Fig. 1 **a** Magnetic field pulse profile. **b** Departure from a tangent line in the plot of the gradient of the f versus B plots, d f/dB is used to determine H_{c2}. Four plots of the Ni6 data at 1,6, 2.1, 3.1, and 4.0 K temperatures are shown here. *Error bars* are estimated to be <±2 T

about 60 kHz for the Ni6 sample. The field dependence of the PDO frequency measured at different temperatures allows the critical field vs. temperature to be obtained. Based on comparisons with direct four-wire measurements of the resistivity [14, 15], we identify H_{c2} as the point at which the frequency's field dependence becomes dominated by the normal-state magnetoresistance; this is observed as a departure from a tangent line to the field dependence of the normal-state frequency. This criterion is often best assessed using the gradient of the f versus B plots, d f/dB (see Fig. 1b and its caption). Error bars are estimated to be $<\pm 2$ T. Data collected during the falling phase of the pulses were analyzed.

In a second part of the experiment, we measured the sample's magnetization in pulsed fields of up to 65 T, using a compensated, inductive extraction magnetometer probe [57] to determine the irreversibility fields. The irreversibility field (H_{irr}) marks the upper limit of the magnetic field—temperature region where superconductors are useful for power applications and increasing H_{irr} is of great technological interest. The irreversibility field H_{irr} was defined as the onset of reversibility in the $M(H)$ loops. Data were acquired for both magnetic field pulse polarities and were acquired every 2 μs, resulting in over 50,000 data points acquired during each pulse. These magnetization measurements were time intensive and we developed a method of extracting the H_{irr} data from the PDO measurements [58]. Two tangent lines are drawn at the lower field elbows. The intersection of the lines gives us magnetic field values that very closely match the irreversibility fields obtained through the classical magnetization measurements as the onset of reversibility in the $M(H)$ loops.

3 Results and Analysis

Figure 2 shows PDO frequency vs. magnetic field plots at multiple temperatures for the Ni5(LG) and Ni6 samples. Each curve was analyzed separately to determine the upper critical field for the measurement temperature using the method detailed in Fig. 1b and its caption.

Figure 3 shows selected magnetization hysteresis loops for Ni6 sample at different temperatures. The lower critical field is very close to 0 T and magnetic vortices penetrate the sample almost immediately; nevertheless, the irreversibility fields are large especially at low temperatures, suggesting significant vortex pinning mechanism.

Figure 4a–c plots H_{c2} and H_{irr} fields as a function of temperature for the Ni5(LG), Ni5(SG), and Ni6 samples. For the Ni5(LG) and Ni6 samples, we included H_{c2} data obtained from resistivity measurements [14, 15]. The

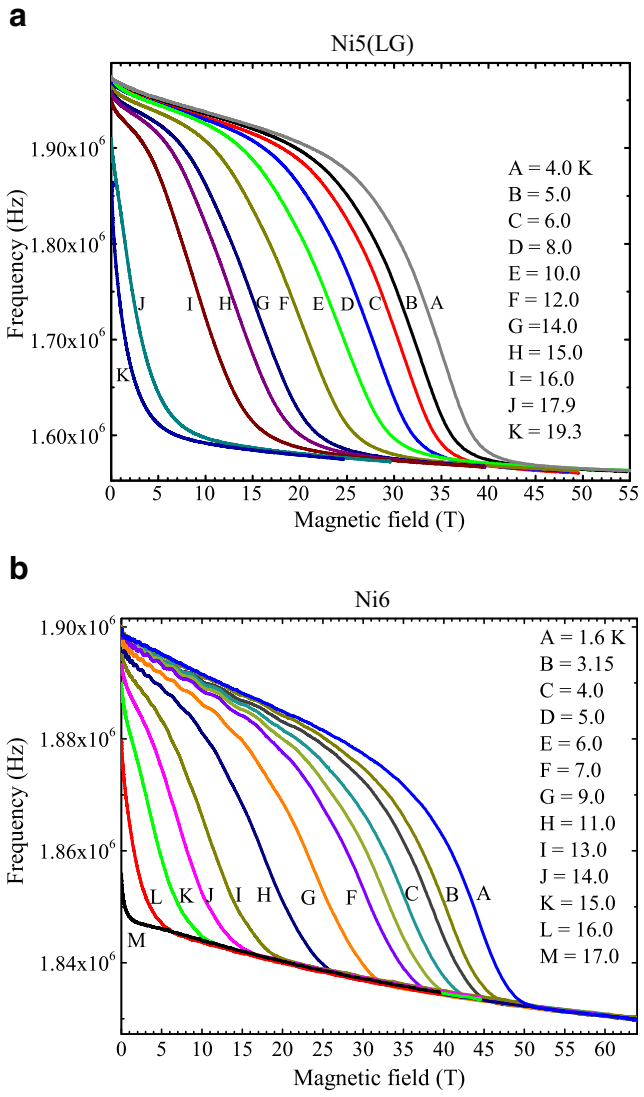

Fig. 2 PDO frequency vs. magnetic field at different temperatures for **a** Ni5(LG) and **b** Ni6 samples

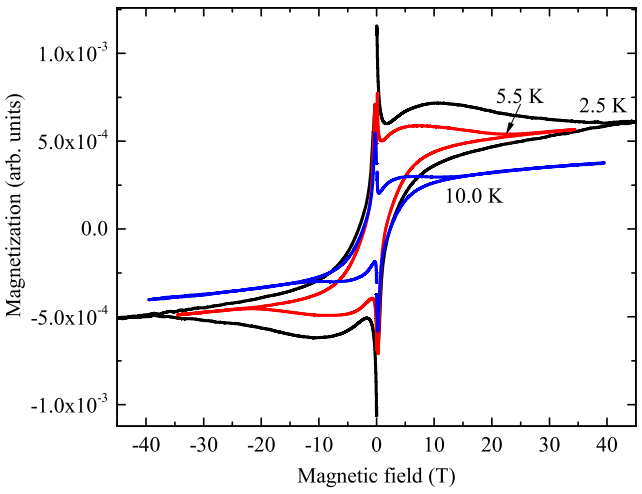

Fig. 3 Selected magnetization vs. magnetic field curves at different temperatures for Ni6 sample

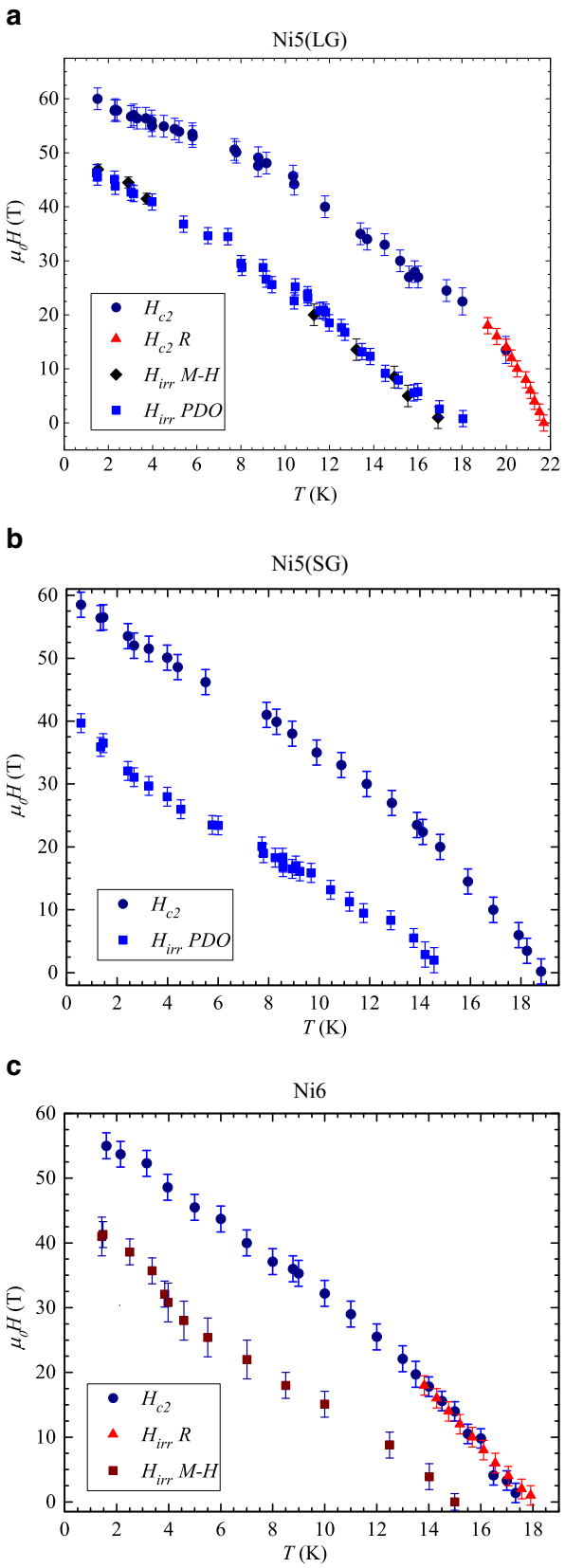

Fig. 4 H_{c2} and H_{irr} as a function of temperature for **a** Ni5(LG), **b** Ni5(SG), and **c** Ni6. H_{c2} is consistently linear near T_c and also appears linear in low temperatures

overlap with H_{c2} data obtained from PDO measurements is excellent, suggesting that this PDO technique is a reliable method of measuring upper critical fields.

The irreversibility line has approximately the same slope as the H_{c2}line but is about 15–20 T below it. The irreversibility field is about 47 T at 1.5 K for Ni5(LG), 40 T at 0.6 K for Ni5(SG), and 41 T at 1.5 K for Ni6. This is excellent for a bulk granular superconductors.

We do not get the concave downward plots seen in typical traditional type II superconductors [51, 59]. Most of the data could be fitted by two different straight lines for each sample. We note the existence of a quite steep increase in the H_{c2} near T_c and the subsequent flattening of the curve at lower temperatures, although this flattening was very moderate for Ni5(SG) and Ni6 samples.

H_{c2}'s almost linear increase near T_c supports the presence of the multiband effect in the system [23]. In light of this, a more complete theoretical description of the H_{c2} curves in various iron pnictides is necessary so that it includes both the multiband orbital and Pauli paramagnetic effects simultaneously.

We observe a noticeable upturn in $H_{c2}(T)$ in low temperatures for the Ni5(SG) sample and, for all samples, linear increase in H_{c2} with decreasing temperature at low temperatures. Several studies showed that $H_{c2}(T)$ exhibits quite a linear increase down to lowest temperatures in 122 compounds, not unlike our results [27, 60, 61].

Ni6 sample shows a little bit of H_{c2} flattening at lowest temperatures. Similar concave shape of $H_{c2}(T)$ curves was observed in 122, 111, and 11 pnictides (122 stands for $BaFe_2As_2$, 111 for AFeAs, where A is a metal such as Na, Li, etc., and 11 for $FeSe_{1-x}Te_x$) [8, 21, 23–25, 27–31]. This $H_{c2}(T)$ flattening suggests strong Pauli limiting of H_{c2}, and indicates that these materials are candidates for the FFLO transition [10, 11, 17–19, 38, 39]. In the possible multi-band structure of these materials, it is possible that FFLO could develop in only one of the bands.

We determine dH_{c2}/dT at T_c and find that Ni5(LG) has the steepest slope of −7.1 T/K among our samples (Table 1). This is one of the larger reported magnitudes for 122, iron-based superconductors [23–26]. This steepest slope at T_c also correlates with the highest measured H_{c2}(1.5 K) and H_{irr}(1.5 K) among our samples. The orbital-limiting field for a BCS superconductor with a single active band is determined by applying $H_{c2}^{orb}(0) = -0.693 T_c (dH_{c2}/dT$ at $T = T_c$) [10, 11]. See Table 1. The calculated $H_{c2}^{orb}(0)$ values, as high as 99.9 T for Ni5(LG), are much larger than the observed values ranging between 55 and 60 T. This suggests that the low-temperature H_{c2} is predominantly a Pauli-limited upper critical field.

We calculate the expected Pauli-limiting field for a weakly coupled BCS superconductor, above which the pair-breaking Zeeman energy exceeds the binding energy of the

Table 1 Summary of the results

Sample	T_c(K)	H_{c2} at 1.5 K (T)	H_{irr} at 1.5 K (T)	$\frac{dH_{c2}}{dT}\Big\vert_{T=T_c}$ (T/K)	$H_{c2}^{orb}(0)$ (T)	$H_{c2}^{P}(0)$ (T)	α	λ_{SO}	H_{c2}/H_{c2f} at 1.5 (K)	τ_{SO} (s)	H_{c2}/T_c (T/K)	t_{break}	ξ at 1.5 K (nm)
Ni5(SG)	19.2	57.5	37.5	−5.9	78.12	35.3	3.2	2.5	1.15	$1.7\ 10^{-14}$	3.0	0.29	2.4
Ni5(LG)	20.4	60.0	47.0	−7.1	99.9	37.5	3.2	2.0	1.06	$2.0\ 10^{-14}$	2.9	0.15	2.3
Ni6	18.5	55.0	41.0	−6.1	77.9	34.0	3.1	3.7	1.11	$1.2\ 10^{-14}$	3.0	0.28	2.4

Cooper pair, as $H_{c2}^{P}(0) = 1.84T_c$. It is much smaller than the predicted $H_{c2}^{orb}(0)$ as well as the experimental H_{c2}(1.5 K) (Table 1). This observation implies that the spin paramagnetic effect may play an important role in determining H_{c2} in this 122 system and that a mechanism to enhance the Pauli limiting field beyond the BCS theory might be necessary. The results are also consistent with calculations showing that in anisotropic superconductors the FFLO state might lead to an enhancement of the upper critical field H_{c2} to between 1.5 and 2.5 times the Pauli paramagnetic limit [40, 42].

We note the relatively high Hc2's compared to their Tc's. Table 1 shows that the H_{c2}/T_c ratio is as large as 3.0 for Ni5(SG) and Ni6. This is significantly higher than comparable ratios for bulk cuprates. The excellent H_{c2}/T_c properties make these bulk materials very promising for applications at liquid helium temperatures.

In order to examine the shape of the temperature dependence of the upper critical field, we apply the WHH approach described earlier. We first notice that the sum over the Matsubara frequencies can be evaluated exactly leading to

$$f(t,h;\alpha,\lambda_{so}) = +\ln 4t + \frac{4\alpha^2h^2-\lambda_{so}^2-i\lambda_{so}\sqrt{4\alpha^2h^2-\lambda_{so}^2}}{8\alpha^2h^2-2\lambda_{so}^2}\psi'([2h+\lambda_{so}+2t - i\sqrt{4\alpha^2h^2-\lambda_{so}^2}]/4t) + c.c. \quad (4)$$

where $\psi'(z) = d^2\ln\Gamma(z)/dz^2$ is the first derivative of the digamma function. Furthermore, near the zero-field critical point (and within the WHH assumptions), the function simplifies to

$$f(t\to 1, h\to 0;\alpha,\lambda_{so}) \to \frac{\pi^2}{4}h + (1-t)\,. \quad (5)$$

Introducing scattering-independent dimensionless field

$$h' \equiv \alpha h = eH_{c2}/2\pi T_c m \quad (6)$$

we notice that the Maki parameter, α, is determined primarily by the high temperature data near the critical temperature, where

$$h' \approx 4\alpha\frac{1-t}{\pi^2}. \quad (7)$$

The spin-orbit scattering parameter, λ_{so}, on the other hand, is primarily set by the lower temperature flattening region of the $h'(t)$ curve (see Appendix for further details).

In Fig. 5a–c, we plot dimensionless critical field h' as a function of $t = T/T_c$ and fit the data. The fitting procedure results in $\alpha = 3.2$ and $\lambda_{so} = 2.0$ for Ni5(LG), $\alpha = 3.2$ and $\lambda_{so} = 2.5$ for Ni5(SG), and $\alpha = 3.1$ and $\lambda_{so} = 3.7$ for Ni6 shown in Fig. 5a–c where we plot h' vs. t with the corresponding $f(t,h;\alpha,\lambda_{so}) = 0$ curves. Table 1 summarizes the results. The impact of different Maki and spin scattering parameters on the shape of the fitted curve is discussed in the Appendix where the structure of the WHH solution is discussed in details.

The noticeable upturn in $H_{c2}(T)$ at low temperatures, can not be explained via λ_{so} and α dependence of the $f(t,h;\alpha,\lambda_{so}) = 0$ curve if we assume the same homogeneous phase at all temperatures below T_c. These data suggest an emergence of a new phase (see Appendix). Gurevich [12, 13] generalizes the WHH calculations to incorporate finite-Q FFLO state, and predicts a sudden increase of H_{c2} at low temperatures—the same linear upturn appears in our low-temperature data. However, multiple unknown parameters of that multi-band description makes fitting impractical in our case.

The higher-temperature, upper critical field H_{c2} data is well described by the WHH model for all samples. Surprisingly, the one-band WHH model also describes the low-temperature behavior of Ni5(LG) sample down to a $t = T/T_c$ of about 0.15 (Fig. 5a). For the Ni5(SG) and Ni6 samples, the experimental data suddenly depart from the fitted WHH curve at a reduced temperature $t$of about 0.29 and 0.28. This low-temperature breakdown of WHH is expected; according to WHH, linear upturn in h' at low t is impossible (see Appendix). The derivative is always smaller by absolute value as we get to lower t.

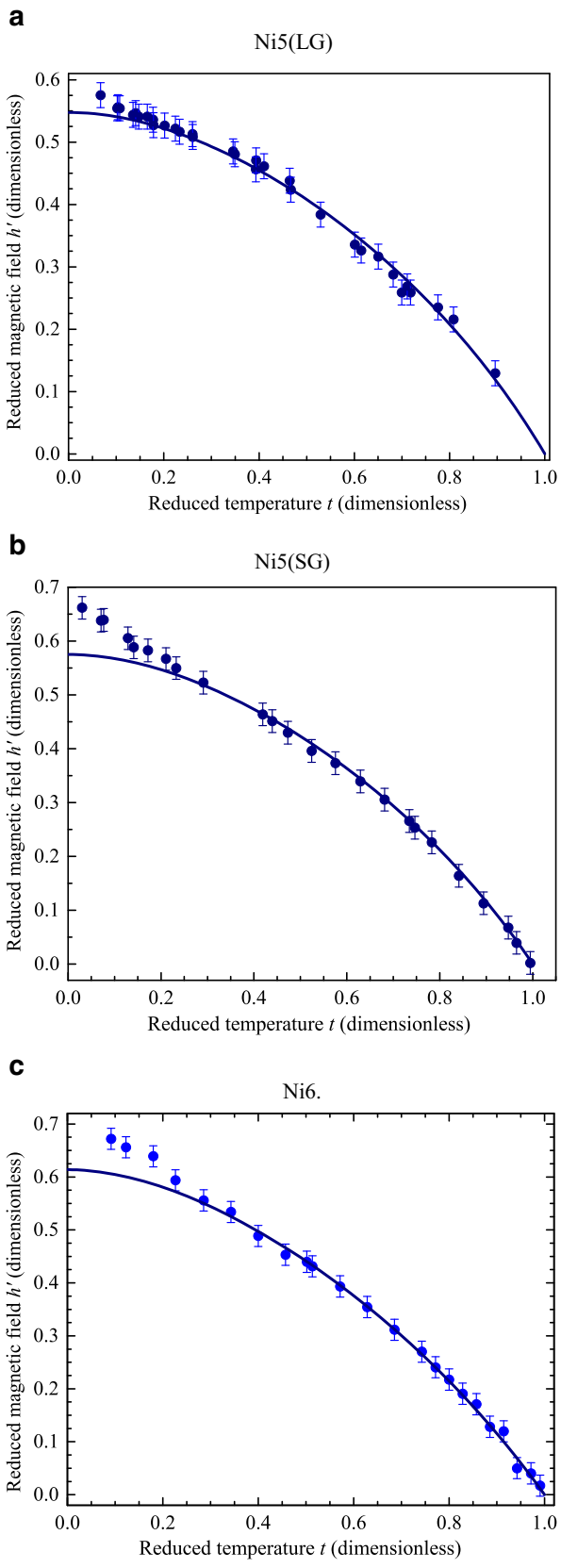

Fig. 5 WHH fit of reduced magnetic field h' versus reduced temperature t for **a** Ni5(LG), using $\alpha = 3.2$ and $\lambda = 2.0$, **b** Ni5(SG), using $\alpha = 3.2$ and $\lambda = 2.5$, and **c** Ni6, using $\alpha = 3.1$ and $\lambda = 3.7$

We determine the enhancement of our H_{c2} data relative to the WHH fitted H_{c2f} at T = 1.5 K by calculating H_{c2}/H_{c2f} and note that the enhancement ratio varies between 1.06 (Ni5(LG)) and 1.15 (Ni5(SG) and the one band fit is close to the measured values (Table 1).

The presence of the Maki parameter α describing the Pauli-limiting effect in the WHH scheme is essential to describe much smaller $H_{c2}(0)$ values than is expected for the orbital-limiting field. The large value of α indicates that the Zeeman pair breaking dominates over the orbital pair breaking and spin-paramagnetic pair-breaking effect is significant. Furthermore, the large value of α(3.1 and 3.2) is comparable to that for CeCoIn5 and organic superconductors that have shown the first-order transition in H_{c2},forming a Fulde-Ferrell-Larkin-Ovchinnikov FFLO-like state [62, 63].

The Appendix shows correlation between the Maki parameter α and $h'(0)$; $h'(0)$ increases, with α and Zeeman pair breaking domination over the orbital pair breaking and spin-paramagnetic pair-breaking effect seems important for enhancing H_{c2} here. This brings out the question how this can be achieved. Studies show that the Maki parameter is enhanced for disordered systems and perhaps that is an important direction of future study [64, 65].

The obtained spin orbit scattering constants indicate that spin-orbit scattering needs to be included in describing the $H_{c2}(T)$ data. In the Ni-doped pnictides, starting from the parent compound, λ_{so} decreases upon doping, due to the reduction in scattering from magnetic excitations as the system moves away from the long-range ordered AFM phase; λ_{so} then reaches a minimum at optimal doping (Ni5(LG)), and begins to increase in the over doped region, possibly due to scattering from magnetic Ni impurities [35].

The spin orbit scattering constant $\lambda_{so} = h_{bar}/(3\pi k_B T_c \tau_{so})$ accounts for the spin-orbit and spin-flip scattering with τ_{so} as the mean free scattering time [35]. We determine τ_{so} for each sample. It ranges from 1.2 10^{-14} s for Ni6 (lowest T_c) to 2.0 10^{-14} s for Ni5(LG) (highest T_c). Measurement of $H_{c2}(T)$ also allows us to find the coherence length $\zeta(T) = \sqrt{\phi_0/2\pi H_{c2}(T)} = 2.3$ nm at T = 1.5 K for Ni5(LG), and 2.4 nm for Ni5(SG) and Ni6, respectively (Table 1).

4 Conclusion

Radio frequency proximity detector oscillator induction technique inpulsed fields up to 65 T was applied to measured the upper critical and irreversible magnetic fields of $Ba(Fe_{0.95}Ni_{0.05})_2As_2$(LG) and (SG), and $Ba(Fe_{0.94}Ni_{0.06})_2As_2$ polycrystalline bulk pnictide superconductors. Full $H - T$ phase diagrams down to a lowest temperature of 1.5 K were obtained.

The higher-temperature, upper critical field H_{c2} data is well described by the WHH model for all samples. We

observe a linear increase in H_{c2} with decreasing temperature at low temperatures as the data departs from the fitted WHH curve in low temperatures, suggesting an emergence of a new phase that can be attributed to the FFLO state. The fitted values of Maki parameter (>1) indicate that the Zeeman pair breaking dominates over the orbital pair breaking and spin-paramagnetic pair-breaking effect is significant. The obtained spin orbit scattering constants indicate that spin-orbit scattering needs to be included in description of the $H_{c2}(T)$ data in these materials.

Both, the higher-temperature behavior, as well as the low-temperature FFLO curve, can be potentially described within a single-band model WHH with added finite-Q dependence (Q is a wave vector of FFLO oscillations) to introduce FFLO instability as described by Gurevich [9, 12, 13]. In this case, possible multi-band structure of these materials could be lumped into effective parameters of the single-band model. However, if FFLO develops in only one of the bands, the expanded influence on the form of H_{c2} is lesser and the upturn in the H_{c2} data in low temperatures is smaller. Anisotropy in the behavior of the upper critical field also plays a role in the explanation of the data, as we see some kind of H_{c2} averaging of different granular orientations. In light of this, a more complete theoretical description of the H_{c2} curves in various iron pnictides is necessary so that it includes both the multiband orbital and Pauli paramagnetic effects simultaneously.

The irreversibility fields were surprisingly high, up to 47 T at 1.5 K, for the Ni5(LG) sample, and showed linear-like increase with decreasing temperature. This magnetic field performance and excellent H_{c2}/T_c properties makes these bulk pnictide superconductors promising candidates for the long sought after superconductivity applications at liquid helium temperatures.

Acknowledgments A portion of this work was performed at the National High Magnetic Field Laboratory, which is supported by National Science Foundation Cooperative Agreement No. DMR-1157490, the Department of Energy and the State of Florida.

Appendix

Here, we investigate the structure of equation

$$f(t, h; a, \lambda_{so}) = 0, \tag{A1}$$

describing the relation between critical field H_{c2} and other parameters, with $f(t, h; a, \lambda_{so})$ given by (4). The natural dimensionless critical field, h, as follows from the WHH theory, incorporates overall mean free time and, hence, α. This is not convenient for fitting experimentally obtained $H_{c2}(T)$ data points because both overall and spin-orbit mean free times (entering via α and λ_{so}) are unknown and must be obtained as the result of the fit. To overcome this difficulty and design an intuitive fitting procedure, we rescale experimental data points $H_{c2}(T)$ with critical temperature, available for each sample, and fundamental dimensional constants, i.e., we use $t = T/T_c$ and $h' = \alpha h = eH_{2c}/2\pi m T_c$, as defined in (3) and (6).

Equation A1 cannot be solved for h' explicitly and we use numerical (secant) method to find h'. In order to make the two-parameter fitting stable, we first investigate how $h'(t)$ changes as a function of α and λ_{so} independently. Figure 6 shows how $h'(t)$ curve changes as a function of α for $\lambda_{so} = 0$, that is when spin orbit interaction is ignored and only disorder scattering is present. At small values of t the curve saturates as a function of t and also as a function of α, developing a noticeable depression as α increases. This shows that, while $h'(t \to 0)$ is increasing with α for small values of α, this nearly linear increase cannot be used to elevate h' at $t = 0$ beyond 0.25 significantly. On the other hand, we also notice that near the zero-field critical temperature, at $t \to 1$, the slope of the $h'(t)$ curve increases (in magnitude) nearly linearly for the whole range of shown values of α.

Clearly, $h'(t)$ curves with $\lambda_{so} = 0$ cannot describe the experimental data shown in Fig. 5. In order to investigate the role of λ_{so} and, hence, τ_{so}, we first plot $h'(t)$ for some small value of α, e.g., 0.4, and vary λ_{so} from 0.0 to 4.0 in increments of 0.4, as shown in Fig. 7. We see that the variation of the curve is rather insignificant for the whole range of t, including $t \to 0$, and is clearly negligible near $t \to 0$. While the latter remains to be the case for larger values of α, the variation of h' near $t \to 0$ is dramatically different for larger values of α, as shown in Fig. 8.

From Figs. 6, 7, and 8, we see that near the zero-filed critical temperatures, at $t \to 0$, the spin orbit mean free time enters as a higher order change as opposed to α, describing overall disorder scattering. This can also be verified analytically as shown in (7). Due to this fact, we can first do

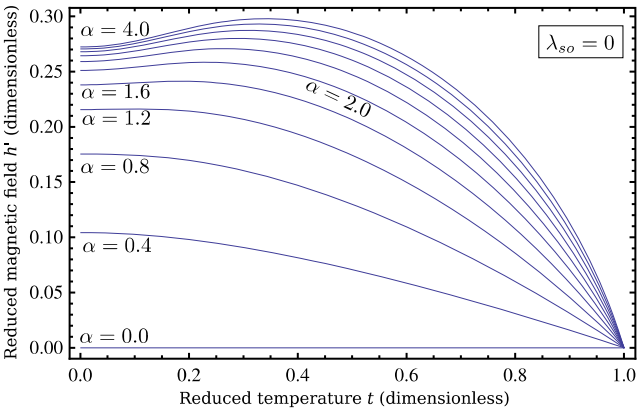

Fig. 6 Plot of h' vs. t for $\lambda_{SO} = 0$ and increasing α from 0 to 4.0 in increments of 0.4

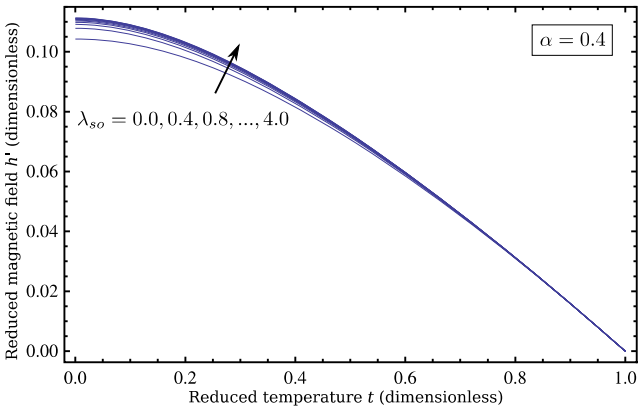

Fig. 7 Plot of h' vs. t for $\alpha = 0.4$ and increasing λ_{SO} from 0 to 4.0 in increments of 0.4

a single-parameter fit for high temperature data do determine the overall scattering mean free time, i.e., parameter α, keeping $\lambda_{so} = 0$. Then, low-temperature data points can be used to determine λ_{so} using the value of α defined by the previous fit. Because both fits are single-parameter fits, the procedure becomes more straightforward and accurate. Furthermore, it provides intuition on the scope of the WHH solution, on which we comment below.

Figure 5b, c clearly demonstrates that the low-temperature experimental data deviates significantly from the WHH description and cannot be described by as single $h'(t; \{\alpha, \lambda_{so}\})$ curve. The initial increase of h' near $t \to 0$ requires a specific value of α, while lower-temperature data points need specific λ_{so}. This leaves several possibilities described in the main text: (i) the low-temperature H_{c2} data describe a different superconducting phase that occurs first where the data deviates from the WHH $h'(t)$ fit; (ii) the data describes critical field of several domains (or sets of domains) with different domains entering superconducting regime at different field.

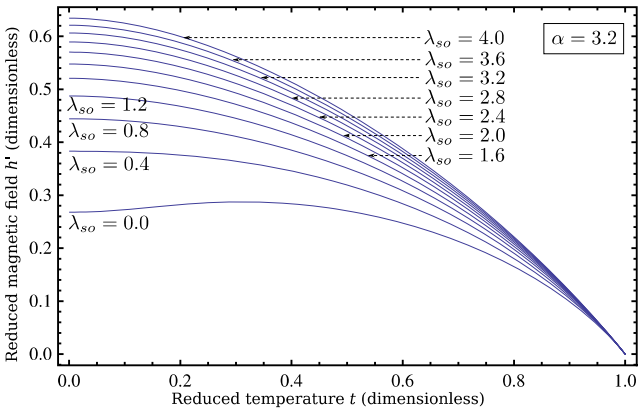

Fig. 8 Plot of h' vs. t for $\alpha = 3.2$ and increasing λ_{SO} from 0 to 4.0 in increments of 0.4

In the latter case, the first set of domains to become superconducting can potentially induce superconductivity in the rest of the sample due to proximity effect. This means that the low-temperature data should also be describable by WHH $h'(t)$ curve or curves. However, those curves must be based on different T_c, α, and (or) λ_{so}. From the above analysis of the $h'(t)$ curves, we see that this necessarily requires lower T_c and larger λ_{so} or α (or both). Furthermore, because WHH $h'(t)$ curves always saturate at $t \to 0$, a single "leading set" of domains may not be enough to fit the data points. These low-T fits cannot be separated into two single-parameter fits described above because $t \to 1$ data due to those domains is inaccessible. The two-dimensional fits become substantially less accurate given the available portion of low-T data. For this reason, we do not show them here.

In case (i), the data appears to replicate features suggested in refs. [12, 13], specifically, the linear upturn of the critical field at $t \to 0$ due to FFLO phase. However, that model would require an unstable multi-dimensional fit, since most of the parameters in that multi-band description are unknown. For this reason, we do not use that model here to fit the obtained data.

References

1. Day, C.: Physics today, 36 august (2009)
2. Wikipedia.org/wiki/Ferromagnetism
3. Tanatar, M.A.: Phys. Rev. B **79**, 094507 (2009)
4. Jaroszynski, J., et al.: Phys. Rev. B **78**, 064511 (2008)
5. Chen, Y.L., et al.: Supercond. Sci. Technol **21**, 115014 (2008)
6. Khasanov, A., Bhargava, S.C., Stevens, J.G., Jiang, J., Weiss, J.D., Hellstrom, E.E., Nath, A.: J. Phys. Condens. Mat **23**, 202201 (2011)
7. Celentano, G., et al.: IEEE Trans. Appl. Supercond 4(3) (2011)
8. Yamamoto, A., Balicas, L., Jaroszynski, J., Tarantini, C., Jiang, J., Gurevich, A., Larbalestier, D.C., Jin, R., Sefat, A.S., McGuire, M.A., Sales, B.C., Christen, D.K., Mandrus, D.: Appl. Phys. Lett. **94**, 062511 (2009)
9. Gurevich, A.: Annual. Rev. of Cond. Matter Phys. **5**, 35–56 (2014)
10. Helfand, E., Werthamer, N.R.: Phys. Rev. **147**, 288 (1966)
11. Werthamer, N.R., Helfand, E., Hohenberg, P.C.: Phys. Rev. **147**, 295 (1966)
12. Gurevich, A.: Phys. Rev B **82**, 184504 (2010)
13. Gurevich, A.: Phys. Rev. B **67**, 184515 (2003). Physica C, 456,160 (2007)
14. Nikolo, M., Shi, X., Jiang, J., Weiss, J.D., Hellstrom, E.E.: J. of Supercond. and Novel Magn. **27**(9), 1983–1990 (2014)
15. Nikolo, M., Shi, X., Jiang, J., Weiss, J.D., Hellstrom, E.E.: J. of Supercond. and Novel Magn. **27**(10), 2231–2239 (2014)
16. Zhang, J., et al.: Front. Phys **6**(4), 463–473 (2011)
17. Maki, K.: Phys. Rev. **148**, 362–9 (1966)
18. Sarma, G.: J. Phys. Chem. Solids **24**, 1029 (1963)
19. Grunberg, L.W., Gunther, L.: Phys. Rev. Lett **16**, 996 (1966)
20. Hunte, F., Jaroszynski, J., Gurevich, A., Larbalestier, D.C., Jin, R., Sefat, A.S., McGuire, M.A., Sales, B.C., Christen, D.K., Mandrus, D.: Nature (London) **453**, 903 (2008)
21. Jaroszynski, J., Hunte, F., Balicas, L., Jo, Y.-J., Raiˇcevi´c, I., Gurevich, A., Larbalestier, D.C., Balakirev, F.F., Fang, L., Cheng, P., Jia, Y., Wen, H.H.: Phys. Rev. B **78**, 174523 (2008)

22. Hecher, J., Baumgartner, T., Weiss, J.D., Tarantini, C., Yamamoto, A., Jiang, J., Hellstrom, E.E., Larbalestier, D.C., Eisterer, M.: Supercond. Sci. Technol **29**, 025004 (2016)
23. Khim, S., Kim, J.W., Choi, E.S., Bang, Y., Nohara, M., Takagi, H., Kim, K.H.: Phys. Rev. B, 184511 (2010)
24. Lei, H., Hu, R., Choi, E.S., Warren, J.B., Petrovic, C.: Phys. Rev. B **81**, 094518 (2010)
25. Lei, H., Hu, R., Choi, E.S., Warren, J.B., Petrovic, C.: Phys. Rev. B **81**, 184522 (2010)
26. Lee, H.-S., Bartkowiak, M., Park, J.-H., Lee, J.-Y., Kim, J.-Y., Sung, N.-H., Cho, B.K., Jung, C.-U., Kim, J.S., Lee, H.-J.: Phys. Rev. B **144512**, 80 (2009)
27. Kano, M., Kohama, Y., Graf, D., Balakirev, F., Sefat, A.S., McGuire, M.A., Sales, B.C., Mandrus, D., Tozer, S.W.: J. Phys. Soc. Jpn **78**, 084719 (2009)
28. Kida, T., Matsunaga, T., Hagiwara, M., Mizuguchi, Y., Takano, Y., Kindo, K.: J. Phys. Soc. Jpn **78**, 113701 (2009)
29. Terashima, T., Kimata, M., Satsukawa, H., Harada, A., Hazama, K., Uji, S., Harima, H., Chen, G.-F., Lio, J.-L., Wang, N.-L.: J.Phys. Soc. Jpn **78**, 063702 (2009)
30. Braithwaite, D., Lapertot, G., Knapo, W., Sheikin, I.: J. Phys. Soc. Jpn **79**, 053703 (2010)
31. Fang, M., Yang, J., Balakirev, F.F., Kohama, Y., Singleton, J., Qian, B., Mao, Z.Q., Wang, H., Yuan, H.Q.: Phys. Rev. B **81**, 020509 (2010). R
32. Klein, T., et al.: Phys. Rev. B **82**, 184506 (2010)
33. Cho, K., et al.: Phys. Rev. B **83**(R), 060502 (2011)
34. Mun, E.D., et al.: Phys. Rev. B **83**(R), 100514 (2011)
35. Ghannadzadeh, S., et al.: Phys. Rev. B **89**, 054502 (2014)
36. Yuan, H.Q., Singleton, J., Balakirev, F.F., Baily, S.A., Chen, G.F., Luo, J.L., Wang, N.L.: Nature **457**, 565 (2009)
37. Braccini, V., et al.: Phys. Rev. B **71**, 012504 (2005)
38. Fulde, P., Ferrel, R.A.: Phys. Rev. **135**, A550–63 (1964)
39. Larkin, A.I., Ovchinnikov, Y.N.: Zh. Exp. Teor. Fiz. **47**, 1136–46 (1964). (Engl. Transl. Sov. Phys.–JETP 20 762 (1965)
40. Shimahara, H.: J. Phys. Soc. Japan **66**, 541 (1997)
41. Shimahara, H.: J. Phys. Soc. Japan **67**, 1872 (1998)
42. Buzdin, A.I., Tugushev, V.V.: Zh. Eksp. Teor. Fiz. **85**, 735 (1983). (Engl. Transl. Sov. Phys.–JETP 85 428 (1983))
43. Bianchi, A., Movshovich, R., Capan, C., Pagliuso, P.G., Sarrao, J.L.: Phys. Rev. Lett. **91**, 187004 (2003)
44. Radovan, M., Fortune, N.A., Murphy, T.P., Hannahs, S.T., Palm, E.C., Tozer, S.W., Hall, D.: Nature (London) **425**, 51 (2003)
45. Kumagai, K., Kakuyangi, K., Saitoh, M., Takashima, S., Nohara, M., Takagi, H., Matsuda, Y.: J. Supercond. Novel Magn. **19**, 1 (2006)
46. Kenzelmann, M., Sträsle, T.h., Niedermayer, C., Sigrist, M., Padmanabham, B., Zolliker, M., Bianchi, A.D., Movshovich, R., Bauer, E.D., Sarrao, J.L., Thompson, J.D.: Science **321**, 1652 (2008)
47. Singleton, J., Symington, J.A., Nam, M.S., Ardavan, A., Kurmoo, M., Day, P.: J. of Phys. Condensed Matter **12**, L641–L648 (2000)
48. Uji, S., Terashima, T., Nishimura, M., Takahide, Y., Konoike, T., Enomoto, K., Cui, H., Kobayashi, H., Kobayashi, A., Tanaka, H., Tokumoto, M., Choi, E.S., Tokumoto, T., Graf, D., Brooks, J.S.: Phys. Rev. Lett. **97**, 157001 (2006)
49. Lortz, R., Wang, Y., Demuer, A., Böttger, P.H.M., Bergk, B., Zwicknagl, G., Nakazawa, Y., Wosnitza, J.: Phys. Rev. Lett **99**, 187002 (2007)
50. Yonezawa, S., Kusaba, S., Maeno, Y., Auban-Senzier, P., Pasquier, C., Bechgaard, K., Jerome, D.: Phys. Rev. Lett. **100**, 117002 (2008). J. Phys. Soc. Jpn. 77, 054712 (2008)
51. Annette, J.: Superconductivity, Superfluids, and Condensates (Oxford Master Series in Condensed Matter Physics) Oxford University Press; 1 ed (2004)
52. Rotter, M., et al.: Phys. Rev. B **78**(R), 020503 (2008)
53. Nikolo, M., Shi, X., Choi, E.S., Jiang, J., Weiss, J.D., Hellstrom, E.E.: J. of Low Temp. Phys. **178**, 345–354 (2015)
54. Nikolo, M., Shi, X., Choi, E.S., Jiang, J., Weiss, J.D., Hellstrom, E.E.: Phys. Procedia **67C**, 987–992 (2015)
55. Altarawneh, M.M., Mielke, C.H., Brooks, J.S.: Rev. Sci. Instrum. **80**, 066104 (2009)
56. Ghannadzadeh, S., et al.: Rev. Sci. Instrum. **82**, 113902 (2011)
57. Goddard, P.A., et al.: New. J. Phys. **10**, 083025 (2008)
58. Nikolo, M., Singleton, J., Vivien, S., Zapf, J., Weiss, J.J.D., Hellstrom, E.E.: J. Supercond. Nov. Magn. (2016). Available Online First:http://link.springer.com/article/10.1007/s10948-016-3628-6
59. Tinkham, M.: Intoduction to superconductivity, Courier, 134–135 (2004)
60. Baily, S.A., Kohama, Y., Hiramatsu, H., Maiorov, B., Balakirev, F.F., Hirano, M., Hosono, H.: Phys. Rev. Lett. **102**, 117004 (2009)
61. Khim, S., Kim, J.S., Kim, J.W., Lee, S.H., Balakirev, F.F., Bang, Y., Kim, K.H.: Phys. C **470**, S317 (2010)
62. Lee, I.J., Naughton, M.J., Danner, G.M., Chaikin, P.M.: Phys. Rev. Lett. **78**, 3555 (1997)
63. Radovan, H.A., Fortune, N.A., Murphy, T.P., Hannahs, S.T., Palm, E.C., Tozer, S.W., Hall, D.: Nature **425**, 51 (2003)
64. Fuchs, G., Drechsler, S.-L., Kozlova, N., Bartkowiak, M., Hamann-Borrero, J.E., Behr, G., Nenkov, K., Klauss, H.-H., Maeter, H., Amato, A., Luetkens, H., Kwadrin, A., Khasanov, R., Freudenberger, J., Köhler, A., Knupfer, M., Arushanov, E., Rosner, H., Büchner, B., Schultz, L.: New J. Phys. **11**, 075007 (2009)
65. Fuchs, G., Drechsler, S.L., Kozlova, N., Behr, G., Kohler, A., Werner, J., Nenkov, K., Hess, C., Klingeler, R., Hamann-Borrero, J.E., Kondrat, A., Grobosch, M., Narduzzo, A., Knupfer, M., Freudenberger, J., Buchner, B., Schultz, L.: Phys. Rev. Lett. **101**, 237003 (2008)